

# Design and Manufacture of a Continuous Fiber-Reinforced 3D Printed Unmanned Aerial Vehicle Wing

Dhileep Kumar Jayashankar<sup>1</sup>, Aarthi Devarajan<sup>1</sup>, Guoying Dong<sup>2</sup>, David Rosen<sup>3</sup>

<sup>1</sup>Research Assistant, <sup>2</sup>Research Fellow, <sup>3</sup>Professor  
Digital Manufacturing and Design (DMandD) Centre, Engineering Product Development  
Singapore University of Technology and Design, Singapore

## Abstract

The Markforged Mark Two 3D printer is capable of printing various orientations of continuous fiber reinforcement. An initial study of how the orientation of the fiber influences the strength characteristics (tensile and flexural properties) was conducted. Four combinations of carbon fiber reinforcement orientations were tested, specifically unidirectional, isotropic, concentric and a combination of isotropic and concentric, with the Markforged Onyx matrix material. The results will aid in designing a wing with the optimum fiber configuration that will give the desired mechanical properties based on the forces acting on the wing. Design for Additive Manufacturing (DfAM) concepts and tools will be used to design and manufacture a large UAV wing. Topology optimization, based on a CFD computed pressure distribution, was used to determine geometric regions where carbon fiber reinforcement could be best utilized. From there, a honeycomb structure was designed to ensure stiffness and light weight based on desired densities. A wing section was fabricated using the Mark Two printer to identify the capabilities and limitations of the system in realizing the design objectives.

Keywords: UAV wing, topology optimization, fiber reinforced composites, material extrusion, design for additive manufacturing

## 1 Introduction

Among the various additive manufacturing (AM) processes, the material extrusion (MEX) process has the capability to produce functional parts in a variety of engineering thermoplastics for various applications [1]. In the past decade, 3D printing of composite materials through MEX had received significant attention among researchers. Composite 3D printing is a process of combining multiple materials in an established 3D printing process to improve mechanical and thermal properties such as strength, stiffness, durability and heat resistance[2]. In AM, composites are based on mixtures of matrix materials and reinforcements. Our interest in this work is in fiber reinforced thermoplastics with the matrix materials including ABS, nylon, polycarbonate, and PLA. Thermoplastics possess specific properties like malleability, ductility and low melting point, which make them an excellent fit for AM. Fiber reinforcements, such as continuous carbon fiber, significantly increase strength and stiffness which is important in a variety of applications. Options for reinforcements include short fibers and continuous fibers which could be carbon, Kevlar or glass fiber. Continuous fibers have the ability to form large structural elements that can withstand substantial loads and disseminate forces along the directions of fiber[3]. Ultimately, this property

of fibers provides advantages in strength over traditional thermoplastics, which makes them a promising means of reinforcement in AM to build light-weight parts [4].

However, the manufacturing compatibility of fiber printing is complicated and poses a significant challenge when it comes to mixing the reinforcement with polymer matrix due to control of fiber orientation, void content and low-cost production [5]. Some researchers have identified three possibilities for fiber integration into the part in MEX processes, which are: 1) adding fibers before the printing process, i.e., filaments itself are a composite; 2) adding fibers in the print head, i.e. one extruder with two entries for filaments; and 3) adding fibers in the part, i.e. with two separate extruders for materials (one for matrix and another for reinforcement) [6]. Approach 1) is useful for carbon nanotubes or graphene reinforcements [7]. Our interest is in approach 3) where we use the Markforged Mark Two printer with their Onyx material and continuous carbon fibers. The Onyx material has a nylon matrix and short carbon fibers. Continuous fibers are deposited by a second printhead that can selectively reinforce each layer.

The on-going research in 3D printing (Type 3) is based on how effectively fibers can reinforce thermoplastics to increase the mechanical properties, which play a major role in advancements in both academic research and for commercial products. The most common matrix-reinforcement combinations in fiber printing are Nylon or ABS-carbon fiber, PC-carbon nanotubes, and PLA-graphene [7]. As th detailed evaluation of mechanical properties of additively manufactured Nylon-carbon fiber reinforced composites are very limited to the authors' knowledge, in this work, we attempted to use Markforged Mark II 3D printer to find the mechanical properties of various Onyx-carbon fiber combinations and applied that specific material combination to 3D print a UAV wing structure.

Design for Additive Manufacturing (DfAM) is another paradigm that enables the designers to maximize the product performance through the synthesis of shapes, sizes, hierarchical structures, and material compositions, subject to the capabilities of AM technologies[8]. By implementing process-specific design rules given by part-level DfAM, one can create the product-process design space and achieve the functional optimization of the design[9]. On the other hand, research on Assembly-level DfAM is still at initial phase to redesign the assemblies by taking advantage of AM-enabled capabilities and its design freedom[10]. In assembly-level DfAM, the possibilities of 3D printing functional assemblies, designing novel product architectures, and achieving part consolidation remain under investigation. We applied in designing a lightweight UAV wing structure using DfAM principles.

In this work, we investigated part-level and MEX-specific DfAM rules for designing a lightweight wing structure of a UAV. We explored a sequential product-process design optimization method and implemented the concepts in designing the UAV wing structure. In support of this design project, the tensile and flexural mechanical properties of 3D printed continuous carbon fiber composites were characterized for four different fiber infill configurations. Resulting properties, as well as the capabilities of the Markforged Mark Two system, were utilized in the wing design. At last, this article also discusses about the manufacturing challenges and limitations of fiber reinforced 3D printing.

## 2 Materials and methods

### 2.1 Materials

The materials, such as Onyx (micro carbon fiber filled nylon/mixture of nylon with chopped carbon fiber) and continuous carbon fiber filament (CCF) were purchased from Markforged, United States. The materials had been conditioned in a dry cabinet with humidity level at 25% prior to use to avoid moisture entrapment. The diameter of the Onyx filament and CCF fiber were measured to be 1.7 mm and 0.32 mm. And the density of Onyx and CCF were measured to be 1.2 g/cm<sup>3</sup> and 1.4 g/cm<sup>3</sup> correspondingly.

### 2.2 Manufacturing

The designed parts were fabricated using Markforged 3D printer with different combination of carbon fiber and Onyx matrix. Of the different CF printers available in today's market, Mark One, Two and X7 from Markforged are particularly relevant for a wide range of applications including aerospace, and automobile, etc. In this study, we used the Mark Two 3D printer at the Singapore University of Technology and Design to print the parts as shown in figure 1(a). In the composites world, Markforged coined this fiber printing technology as Continuous Filament Fabrication (CFF), which comes under the category of MEX processes. These printers utilize two nozzles to print the part, one being a thermoplastic nozzle with Onyx (nylon matrix with chopped carbon fiber that also acts as a support material), and another one for carbon, glass or kevlar fiber. The Mark Two printer has a provision to mount a CF filament spool and a separate pelican box for matrix material.

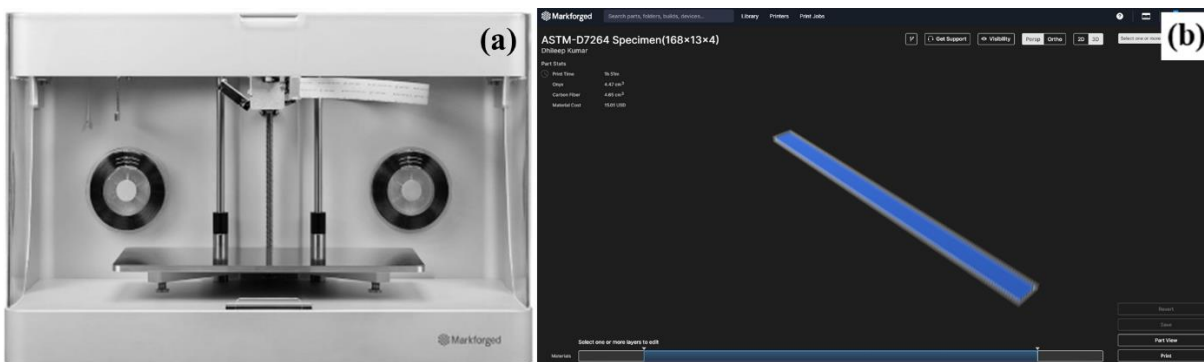










Figure 1 (a) Mark II 3D printer (b) Flexure specimen sliced in EIGER software

The volume fraction of fiber to matrix can be easily controlled by the pre-processing software called EIGER, which is a cloud-based software provided by Markforged that can be used to import, orient and align the geometrical parts in the print bed before printing. The user-machine interface provides the user with two customized fill options, concentric and isotropic infill, in which the user can control the fiber deposition at each layer in a part using customizable fiber angle and orientation options. Within this paradigm, one can combine both concentric & isotropic infill and generate several different fiber configurations in a part based on the performance requirements and cost. In our case, the .STL files were imported in the EIGER software to prepare parts for printing by inducing the fibers at required locations as shown in figure 1(b). The samples were then printed with the predetermined print settings provided by Markforged as there is lack of option for customized print parameters. Throughout the printing, the Onyx nozzle temperature was maintained at 274°C and CCF's nozzle temperature at 254°C. The brim option was enabled in the print settings, and washable glue was applied to the bed plate for part-bed adhesion.

### 2.3 Design of fiber configurations

The orientation of the carbon fiber plays a major role in strength characteristics for both tensile and flexural properties. With the available fiber fill options, we generated four possible combinations of fiber reinforcement by combining both concentric and isotropic fill along with Onyx as shown on Table 1.

Table 1 Fiber Reinforcement Configurations

Specimens	Unidirectional [0°]	Isotropic [0°/45°/90°/135°]	Concentric (4 fiber rings)	Isotropic & Concentric (2 fiber rings)
Code	U	I	C	I_C
Tensile (ASTM D3039 250x25x2.5 mm)				
Flexural (ASTM D7264 168x13x4 mm)				

According to ASTM standards, the sample thickness for tensile test is set to be 2.5 mm with 20 layers of printing, out of which 16 layers are utilized for fiber reinforcement. Similarly, the sample thickness for flexural test is set to be 4 mm with 32 layers of printing, out of which 28 layers are utilized for fiber reinforcement. For the sake of simplification, we represent the samples using codes throughout the article. The naming conventions for the samples are Tensile (T), Flexural (F), Unidirectional (U), Isotropic (I), Concentric (C), and Isotropic & Concentric (I\_C). The sample codes were generated based on the type of test method used followed by the fiber configuration, for example, T\_U represents tensile samples with unidirectional fiber layers. The first configuration, F\_U & T\_U was designed with unidirectional fiber reinforcement, the fibers being oriented at 0° angle at all fiber layers. The second configuration, F\_I & T\_I was designed with isotropic fiber reinforcement, the fibers being oriented at 0°, 45°, 90°, and 135° angles, where each angle takes up an entire layer in the sample. With the isotropic fiber configuration, once the base matrix layers are printed, the first fiber layer would be laid at [0°] angle followed by [45°], [90°] and [135°] at second, third and fourth layers, respectively. The fiber angle pattern [0/45/90/135°] is then repeated at every four layers which in our case is considered as the Isotropic (I) configuration. The third configuration, F\_C & T\_C was designed with concentric fiber reinforcement, four fiber rings [0/90°] being concentrically surrounded from outwards to inwards without isotropic fill. The fourth configuration, F\_I\_C & T\_I\_C was designed with both types of

fiber reinforcement, with isotropic fibers oriented at  $[0/45/90/135^\circ]$  angles in the center of the specimen followed two concentric fiber rings  $[0/90^\circ]$  surrounding them.

The fiber volume fraction for all the configurations was estimated from the Eiger-cloud slicing software provided by Markforged. The calculation is akin to traditional composite structures that follows the rule of mixtures (ROM) method. Since, Eiger software has the ability to compute the required volume of both matrix and fiber material for the part to be printed, the fiber volume fraction was estimated from the software itself and reported at figure 2. However, the experimental study was not conducted for the distribution of voids and porosity.

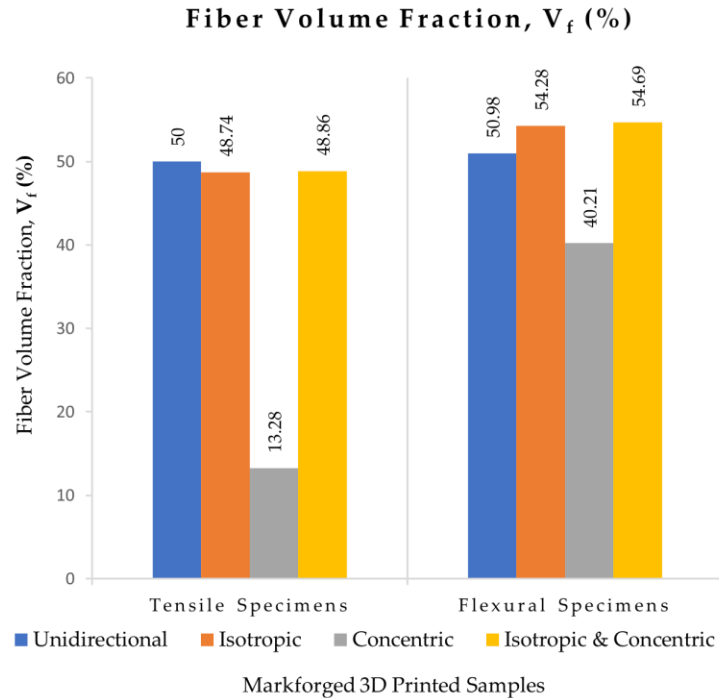


Figure 2 Fiber volume fraction for different fiber configuration

## 2.4 Experimental

### 2.4.1 Tensile test

The test specimens were designed and printed according to ASTM D3039 (Standard Test Methods for Tensile Properties of Polymer Matrix Composite Materials) as shown on figure 2. The dimensions of the specimen were set to be  $25 \times 250 \times 2.5$  mm. Five specimens were 3D printed for each type of fiber configuration. The test was conducted in a double column universal testing machine - 100 kN Instron 5982 (Instron, US). The speed of testing was calculated from the ASTM standards and set to be 1.5 mm/min.

### 2.4.2 Flexural test

The test specimens were designed and printed according to ASTM D7264 (Standard Test Methods for Flexural Properties of Polymer Matrix Composite Materials) as shown on figure 3. Considering the span-to-depth ratio as 32:1 and support span length as 128 mm, the dimensions of the specimen were set to be  $13 \times 168 \times 4$  mm. Five specimens were 3D printed for each type of fiber configuration. The test was conducted in a single column universal testing machine - 1 kN Instron

5943 (Instron, US). The speed of testing was calculated from the ASTM standards and set to be 6.82 mm/min.

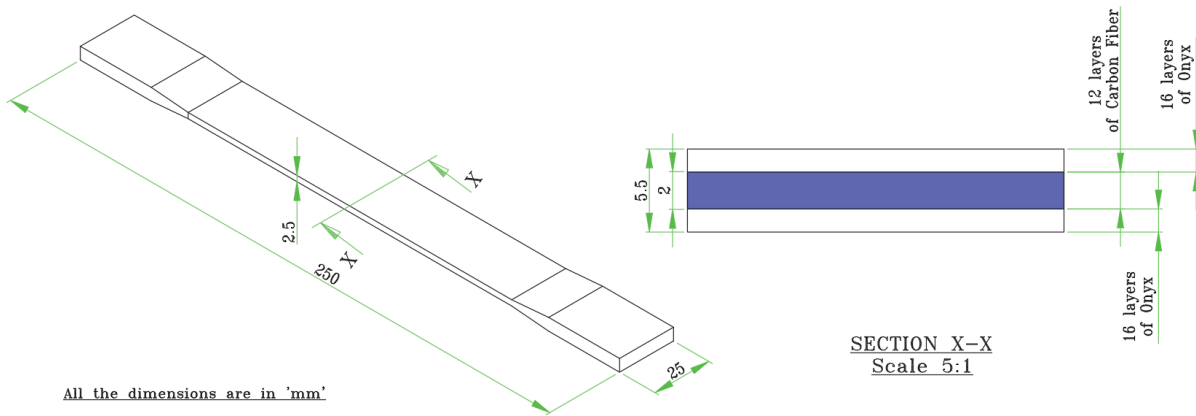


Figure 3 Dimensions of tensile specimen and sectional view to illustrate the fiber and matrix layers

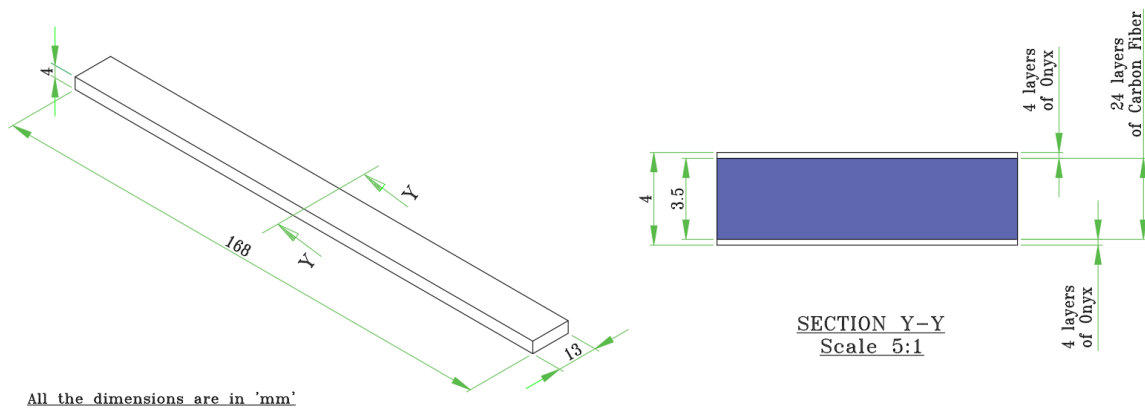


Figure 4 Dimensions of flexural specimen and sectional view to illustrate the fiber and matrix layers

### 2.4.3 Tensile Properties

Figure 4(a-d) shows the typical tensile stress vs strain graph of five specimens in four designed fiber configurations, such as (a) Unidirectional (T\_U), (b) Isotropic (T\_I), (c) Concentric(T\_C) and (d) Isotropic & Concentric (T\_I\_C). It is observed that the unidirectional fiber configuration specimens (T\_U) exhibited higher tensile stress and modulus of elasticity than other fiber configurations with  $523.98 \pm 20.1$  MPa and  $23.59 \pm 0.976$  GPa, respectively. Similar results were reported by Goh et.al [11] but all T\_U coupons broke abruptly due to the brittle nature of the carbon fiber without any drops which contradicts the statement reported by Goh et.al.[11] The rest of the fiber configurations, T\_I, T\_C, and T\_I\_C behaved in a very similar way but with strength and stiffness values nearly half of those for T\_U specimens with the range between 180-230 MPa for maximum tensile strength and 10-14 GPa for modulus of elasticity. T\_U & T\_I specimens exhibited brittle failure and the fracture surface appeared to be fibrous husk where the fibers spread out shortly after the breakage. With brittle failure in T\_U & T\_C specimens, the fiber-matrix

debonding was the primary fracture mechanism as the matrix material was separated from the fiber like a shell as shown on figure 5(b). Interestingly, the fiber-matrix debonding was not observed in T\_C & T\_I\_C specimens during the tensile test.

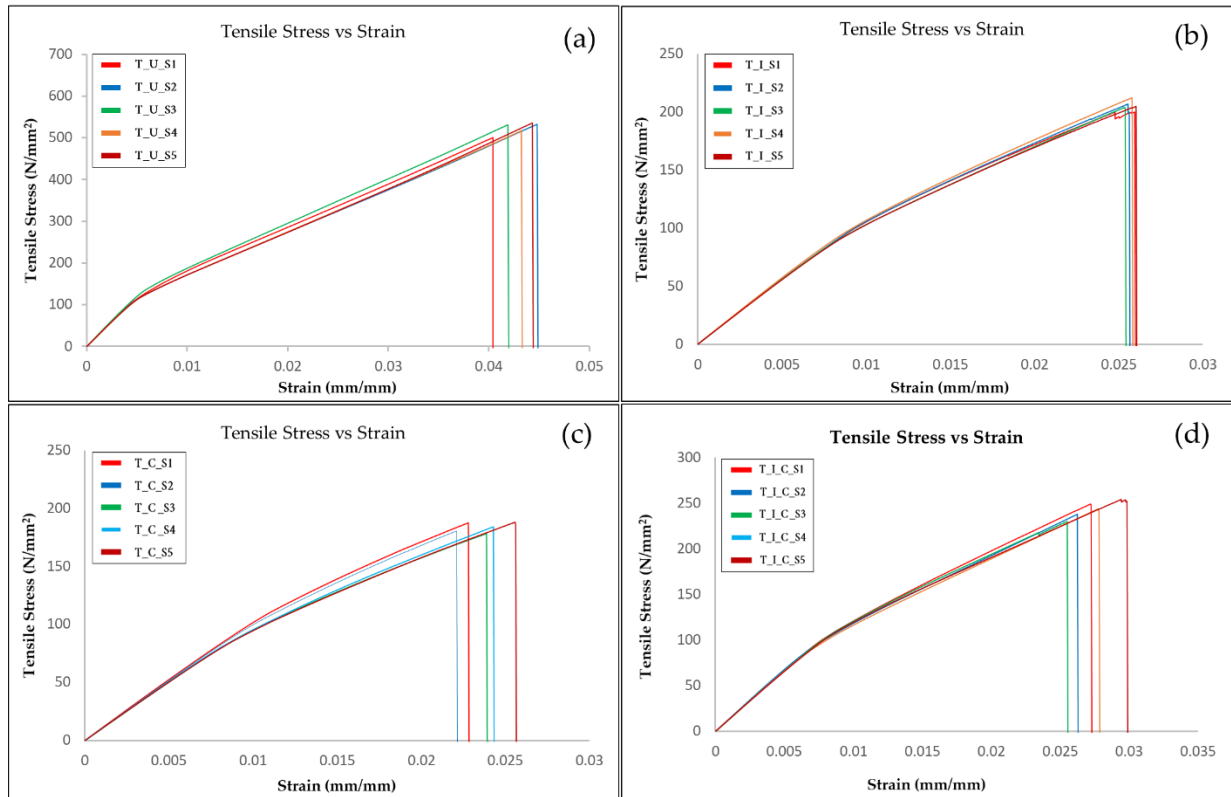


Figure 5 Stress-Strain curve of tensile specimens for (a) T\_U, (b) T\_I, (c) T\_C & (d) T\_I\_C

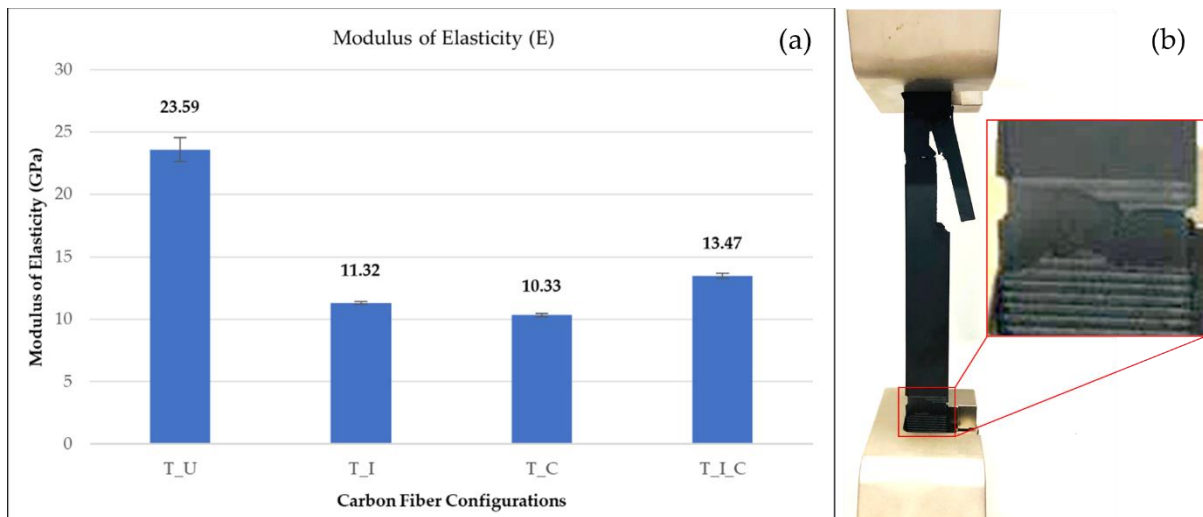


Figure 6 (a) Tensile modulus,  $E_t$ , (b) Brittle failure on tensile specimens(T\_U)

Figure 5(a) depicts the Young's modulus ( $E_t$ ) of the different configurations from tensile tests. Overall, unidirectional specimens possess superior strength and stiffness compared to other

fiber configurations. On the other hand, T\_C configuration produced the lowest tensile strength and modulus with  $182.23 \pm 4.88$  MPa and  $10.33 \pm 0.148$  GPa, respectively.

### 2.4.4 Flexural Properties

Figure 6(a-d) shows the typical flexural stress vs strain graph of five specimens in four designed fiber configurations, such as (a) Unidirectional (F\_U), (b) Isotropic (F\_I), (c) Concentric (F\_C) and (d) Isotropic & Concentric (F\_I\_C). The flexural test results demonstrate that the strength and stiffness of the specimens were greatly affected by the variation of fiber reinforcement and the fiber volume fraction as shown on figure 2. From figure 6(a), it is observed that unidirectional fiber configuration specimens (F\_U) exhibited highest flexural strength and modulus than other fiber configurations with  $352.51 \pm 14.01$  MPa and  $22.97 \pm 0.15$  GPa, respectively. F\_U specimens behaved linearly up to 1.4% flexural strain and failed abruptly as shown on figure 7(b) which is similar to the studies reported by Goh et.al [11]. On the other hand, F\_C & F\_I\_C specimens behaved analogous to F\_U sample until reaching 1.5% strain but with F\_I\_C configuration, it was noted that the samples were not broken even after excessive straining time. Both F\_C & F\_I\_C designs appeared to show successive fiber failure with plastic yielding and based on the stress-strain graph, it is clear that the specimens suffered fiber micro-cracking after 2% strain is achieved. Also, the specimens with high fiber volume fraction achieved significantly higher strength and show low ductility. Surprisingly, the concentric fiber configuration (F\_C) performed well by having only 4 fiber rings with the very low fiber volume fraction of 13.28% as shown in Figure 2. The mechanical properties for different fiber configurations are summarized in Table 2.

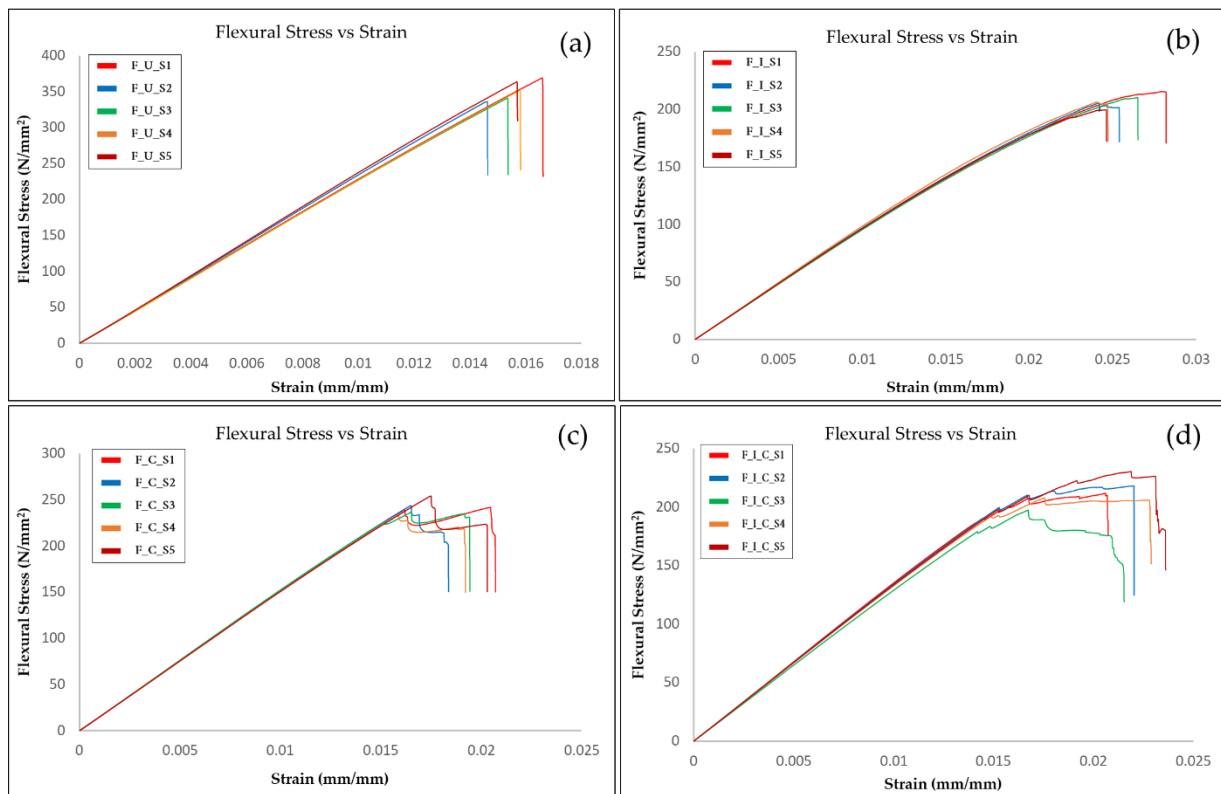


Figure 7 Stress-Strain curve of flexural specimens for (a) F\_U, (b) F\_I, (c) F\_C, (d) F\_I\_C



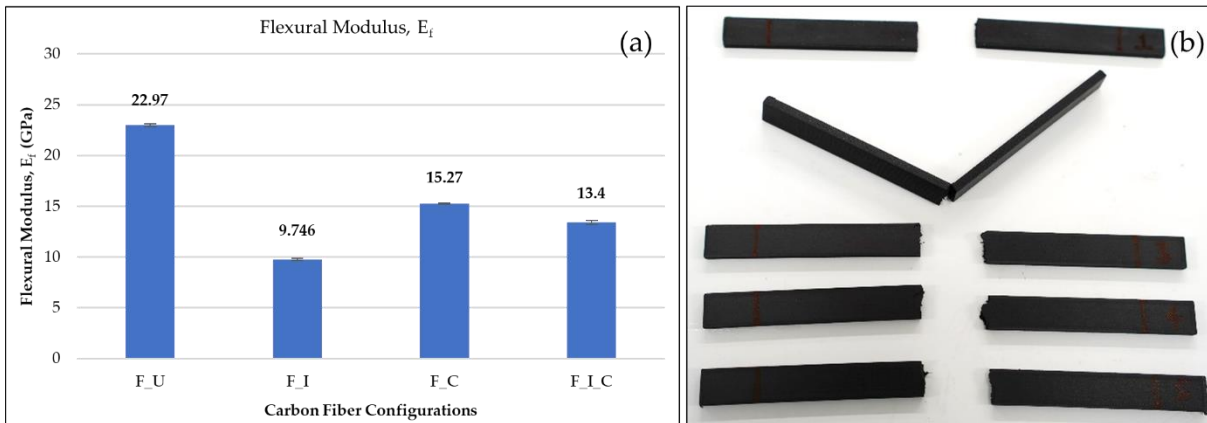


Figure 8 (a) Flexural modulus,  $E_f$  (b) Fractured flexure specimens(F\_U)

Table 2 Mechanical properties of different fiber configurations

Mechanical Properties	Unidirectional [0°]	Isotropic [0/45/90/135°] <sub>s</sub>	Concentric (4 fibre rings)	Isotropic & Concentric (2 fibre rings)
Tensile Strength (MPa)	523.98	205.74	182.23	233.01
Tensile Modulus (GPa)	23.59	11.32	10.33	13.47
Flexural Strength (MPa)	352.51	207.33	241.87	213.11
Flexural Modulus (GPa)	22.97	9.746	15.27	13.4

### 3 Design of Unmanned Aerial Vehicle

#### 3.1 UAV Design

For the purposes of this research, a scale model of the Unmanned Aerial Vehicle (UAV) MQ-9 Reaper (US Airforce, United States), also known as Predator B, was designed in SolidWorks 2020 as shown in figure 9. Since the MQ-9 design is one of the most successful UAV in the last two decades, it was chosen for a better comparison for the proposed design techniques.

Some parts of the design were acquired from several online databases and simplified according to our study as our focus is mainly on optimizing the wing structure. Only one side of the UAV wing structure is considered for this study and to 3D print the full wing structure in the Mark Two, the half-wing was scaled down to 16:1 with the span of 625 mm and the root and tip chord as 90 mm & 45 mm. For the sake of simplicity and in order to demonstrate the design methodology for wing structure involving additive manufacturing, the acquired wing design will act as a supplement for validating the design method.

#### 3.2 Numerical modelling of the UAV wing structure

The ultimate aim of this study is to conduct topology optimization on a wing structure to reduce the mass while maintaining the structural performance and taking advantage of design freedom through additive manufacturing. Numerical studies including computational fluid dynamics (CFD), finite element analysis (FEA) and topology optimization were conducted on the half wing structure of the UAV using SolidWorks 2020 software.

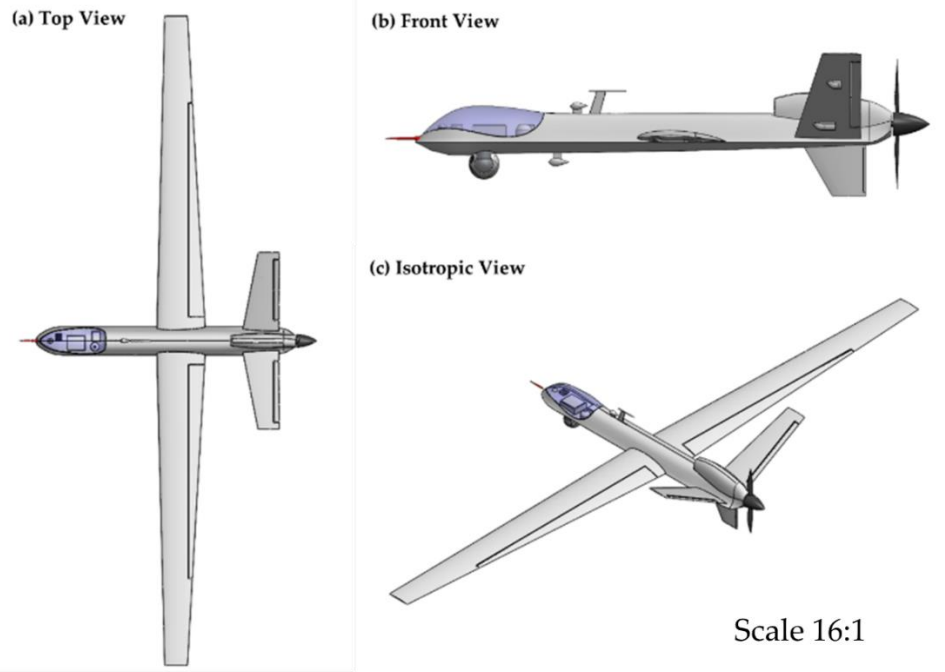


Figure 9 Design of Unmanned Aerial Vehicle (Predator B - MQ-9 Reaper) with a, b, c being top view, front view, and Isotropic view

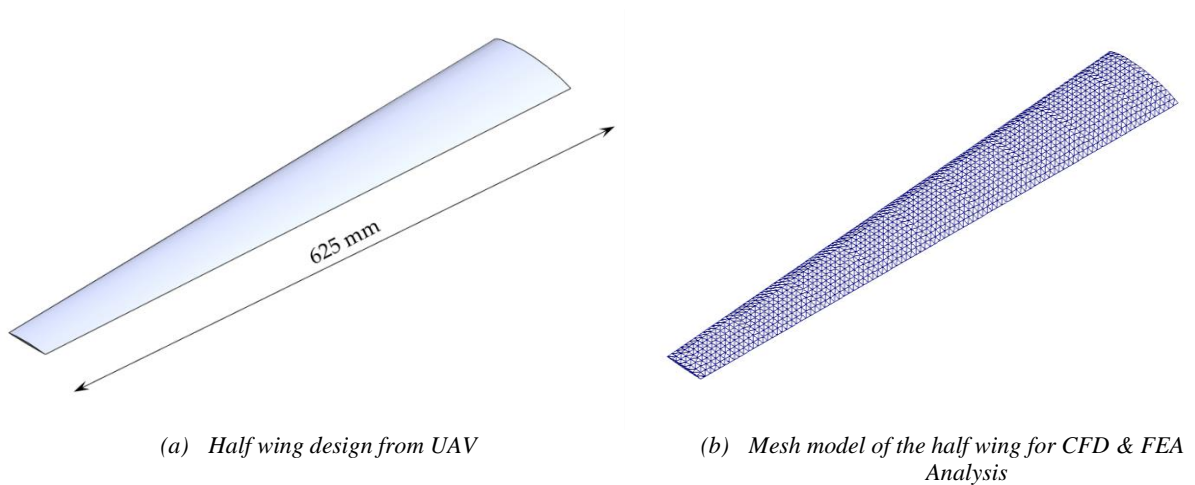


Figure 10 Half wing structure from UAV design

The analysis begins with the CFD of the wing structure and the results from CFD were taken as input loading conditions in the static analysis to calculate von-Mises stresses and displacements, which was then followed by topology optimization. As the velocity of most of the UAV falls between 45-60 m/s, we chose 50 m/s for CFD study, then the results from CFD study in the form of pressure distribution on the wing structure and the gravitational force were considered for the static FEA. At last, the topology optimization study involves the result from both CFD and FEA and the weight optimization parameters were set to 5%, 10% and 15% of the weight of the solid wing structure. The FEA component in SolidWorks was used for the analysis. For the initial studies, only Onyx material was used for the entire wing structure whereas in the

later part Onyx and continuous carbon fiber were used for redesigning the wing. Figure 10(a & b) shows the half wing design from UAV and its SolidWorks mesh model.

## 4 Result & Discussion

### 4.1 Stresses and Finite Element Analysis

The primary objective of the CFD analysis is to find out the dynamic pressure distribution over the wing structure through an input velocity of 50 m/s in x-axis (towards the leading edge). Within SolidWorks, under the CFD domain, the density of air was set to be  $1.225 \text{ kg/m}^3$  and the thermodynamic parameters such as pressure and temperature were set be 101325 Pa and 293.2 K. Furthermore, the thermal wall condition for the analysis is chosen as adiabatic wall with  $5 \text{ }\mu\text{m}$  roughness. Figure 11 shows the CFD results and the pressure distribution over the wing surfaces. As the wing already experiences dynamic loads throughout the leading edge, it is evident that the leading edge needs to be strengthened by introducing carbon fiber in the design. However, no stress and load were spotted at the trailing edge of the wing. From the CFD results, the pressure distribution in 3D space was exported and given as an input loading condition for the static analysis.

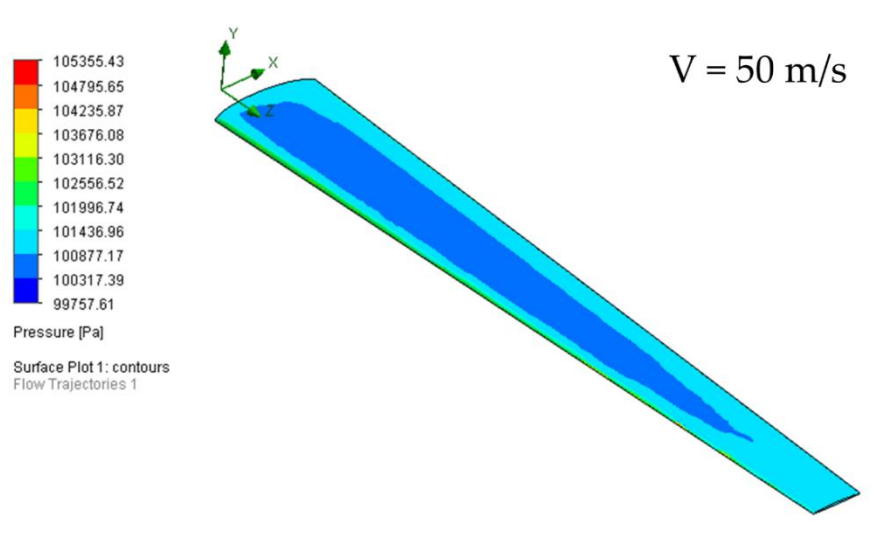


Figure 11 Static loading conditions obtained from computational fluid dynamics (CFD) analysis

Figure 12(a & b) shows the von-Mises stress and displacement of the wing from the static analysis. The maximum stress and displacement experienced by the wing are 2.834 MPa and 61.712 mm. The output of the static study was given as an input for the topology optimization and the wing is optimized for best stiffness to weight ratio for three different weight percentages, 5%, 10% and 15%, as shown on figure 13.

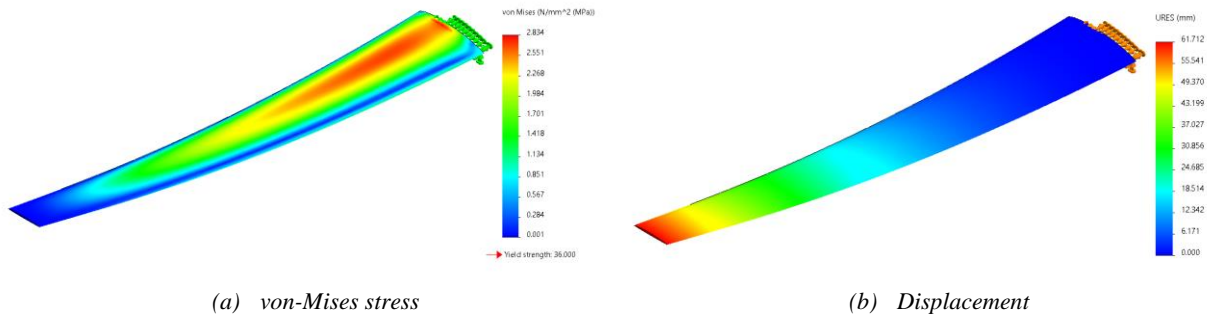


Figure 12 Static analysis of the wing

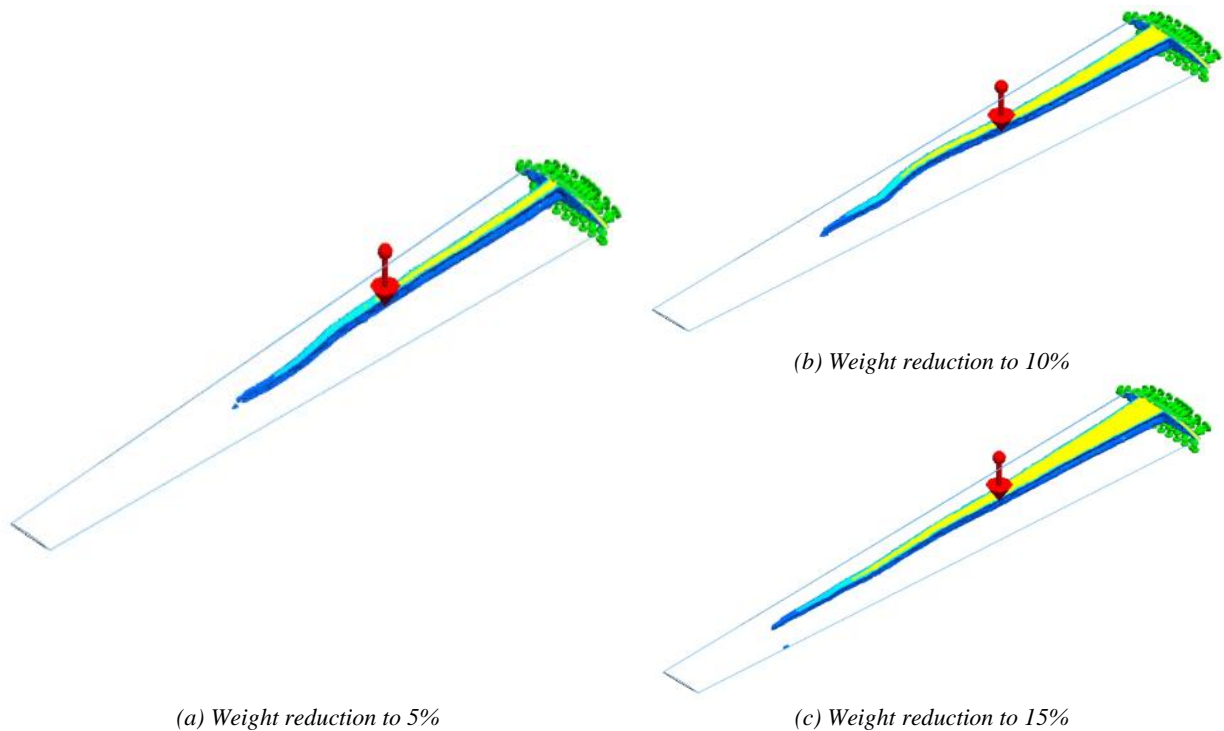


Figure 13 Topology optimization for different weight percentages

Though the mechanical properties of 3D printed carbon fiber composites has been analyzed and evaluated, there are other considerations such as the effect of print process parameters that includes fiber orientation, fiber volume fraction, stacking sequence of fiber ply, matrix infill pattern (such as triangular, rectangular, hexagonal, etc), infill density, raster angle, layer thickness, build orientation (XY, YZ, ZX), printing temperatures (Onyx nozzle temperature, fiber nozzle temperature), and printing speed. Since a process parameter study requires extensive research on fiber composites, it was not included in this study.

#### 4.2 Optimized UAV wing structure

The optimized wing structure was designed in SolidWorks and Rhino software based on the resultant geometric configuration from the topology optimization in which the weight of the wing was reduced to 5% of its original weight. The optimized design was exported and remodeled to incorporate honeycomb design and carbon fiber reinforcement in the wing. Since the final part is subjected to 3D printing, the wing was designed in a way that is compatible to be produced by the

Mark Two machine. The new wing design consists of three parts; namely, (i) Outer shell; (ii) Carbon fiber reinforcement; and (iii) Honeycomb core. Figure 15(a) & (b) offers a closer look of the final wing design with 5% density design in which the outer shell was set to be transparent for the visibility of core and fiber. The fiber was reinforced in the top and bottom sections of the wing that resulted from topology optimization for each of the three different weight percentages shown on figure 13. Additionally, we placed the fibers at the leading edge of the wing as it undergoes high stress as obtained by CFD and static analysis. In contrast, the stress at the trailing edge was comparatively smaller so it was ignored. The carbon fibers were bolstered in the design at  $0^\circ$  orientation as the unidirectional (T\_U & F\_U) fiber placement attained higher strength than other fiber configuration as discussed in section 3.1 and 3.2.

The 2D regular honeycomb core was designed based on the relative density model from cellular solids [12]. For designing the honeycomb core, we developed a computational parametric model in Rhino-Grasshopper software that can compute the side length of the hexagon ( $l$ ) and cell wall thickness ( $t$ ) as shown on figure 14(a) while still maintaining its relative density to 5%. Using the relative density equation (as mentioned below), we found out the ratio of cell wall thickness ( $t$ ) to side length of hexagon ( $l$ ) as 0.0433 by manual calculation. Then,  $t/l$  ratio was given as an input parameter in Rhino-Grasshopper software as shown on figure 14(a) to find out the honeycomb's cell size and cell wall thickness that satisfies the above relation. Once the raw honeycomb is generated in Rhino-Grasshopper, the interior wing profile was designed by leaving sufficient space for both fibers and the outer shell. The interior profile was then imported into Rhino and the actual honeycomb core was cut from the raw honeycomb section using some basic Boolean operations. At last, both the honeycomb core and the outer shell (with the space for fiber reinforcement) was assembled in SolidWorks as shown on figure 14(c).

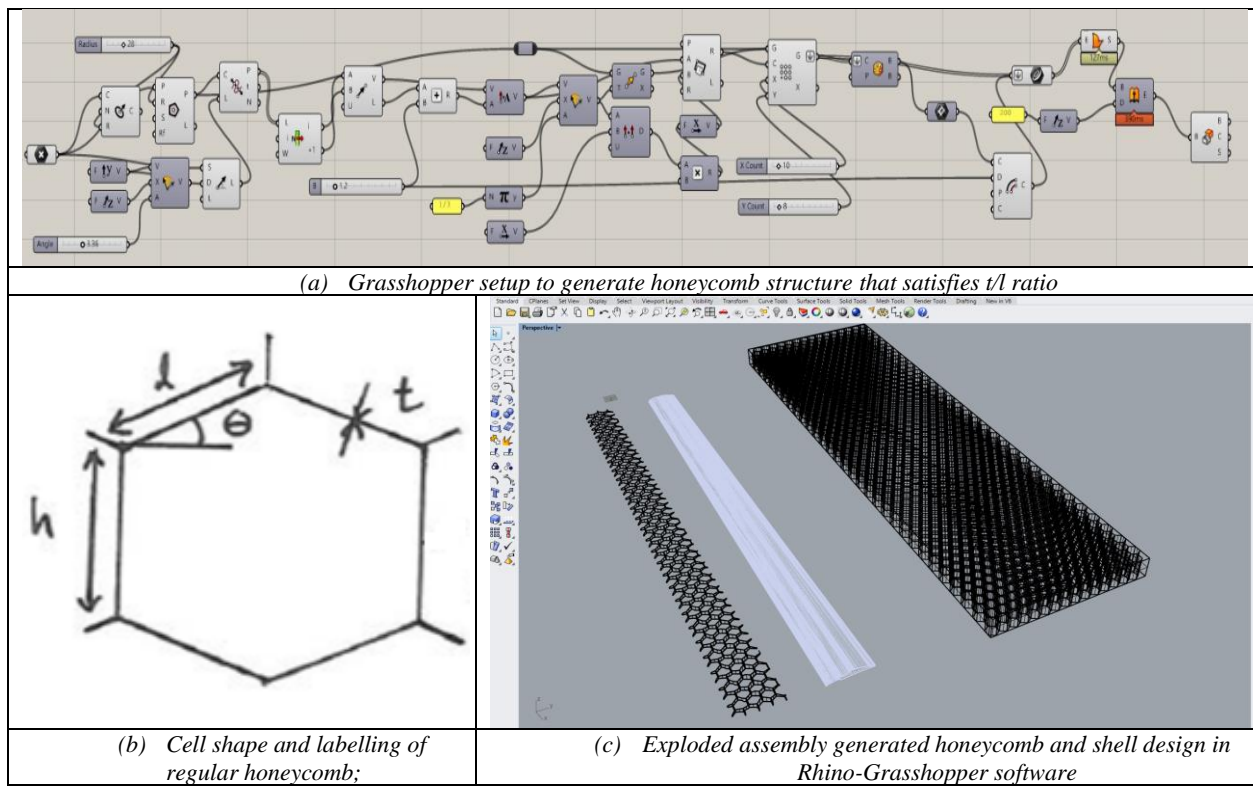


Figure 14 Optimized UAV wing design process

Relative Density,

$$\frac{\rho^*}{\rho_s} = \frac{M_s}{V_T} \cdot \frac{V_s}{M_s} = \frac{V_s}{V_T} = 0.05$$

(volume fraction of solid)

$$\frac{\rho^*}{\rho_s} = \frac{2}{\sqrt{3}} \cdot \frac{t}{l} = 0.05 \Rightarrow \frac{t}{l} = 0.0433$$

(for a regular hexagon)

Where,

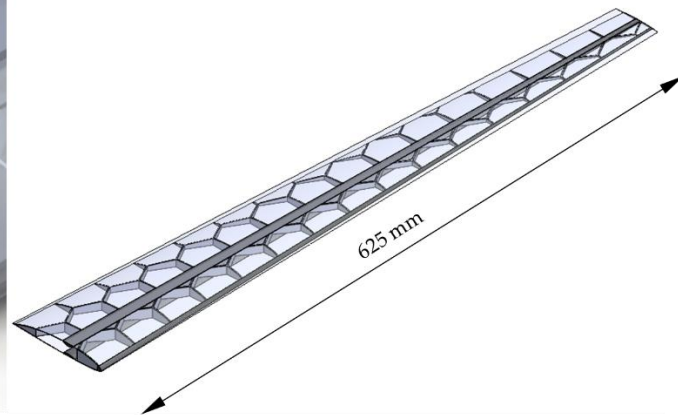
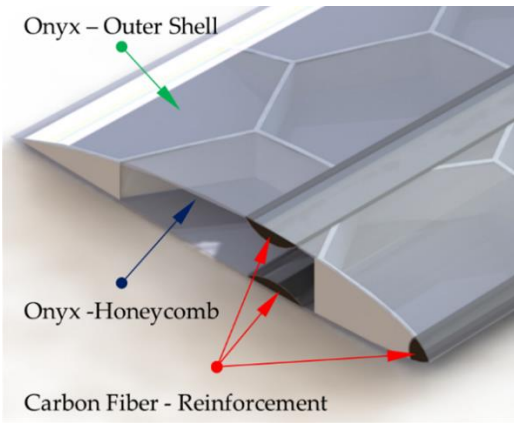
$\rho^*$  = density of cellular structure

$\rho_s$  = density of cellular solid

$M_s$  = mass of cellular structure

$V_T$  = vol of cellular structure

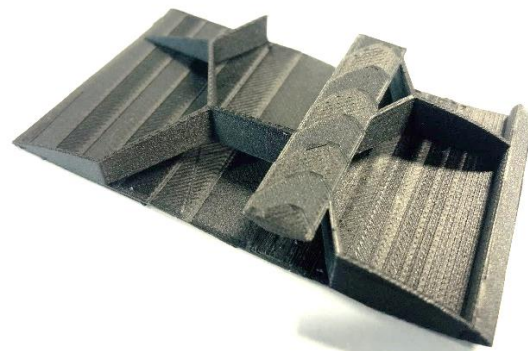
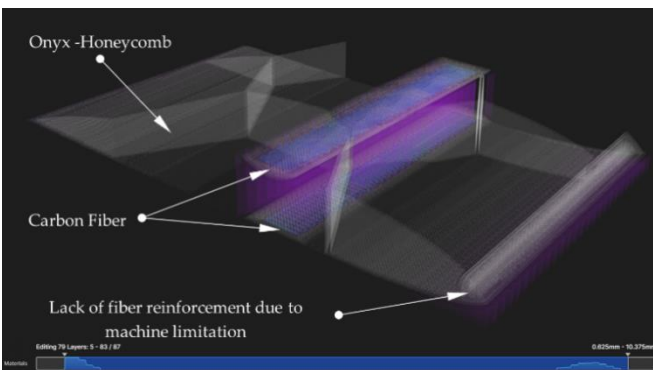
$V_s$  = vol of solid (i.e. without voids)



(a) Optimized wing and assigned the material for 3D printing in Markforged

(b) Optimized wing structure with honeycomb design and carbon fiber reinforcement

Figure 15 Optimized UAV wing design



(a) Small section of final wing design sliced using Eiger cloud slicing software

(b) 3D printed model in Mark II – the top outer skin of the wing was removed for visibility

Figure 16 Optimized UAV wing sliced in EIGER, followed by printing in Markforged Mark II

A small section of the wing model was created and imported in build preparation software-Eiger for visualizing fiber placements and configuring the build for 3D printing. While designing the final wing, we introduced the fiber at the leading edge considering the stresses involved in CFD and static analysis but since the cross section of the fiber at leading edge is relatively small, and possesses a tapered section, the build preparation software failed to fill the fiber in that region

as shown in Figure 16 (a). It became evident that the Markforged system has some limitations that were not known to us. Such issues require users to do more iterations in designing fiber infills. The small section was successfully 3D printed as shown in Figure 16 (b); the top skin was removed so that the internal structures are visible. In the future, we will use our learning about the Markforged system to redesign the fiber reinforcement to properly account for the system's capabilities and limitations.

## 5 Conclusion

The Markforged Mark Two 3D printer is a type of material extrusion system that is capable of printing various orientations of continuous fiber reinforcement. We designed a scale model of a UAV wing to be fabricated using the Markforged system. In support of this design study, we characterized the mechanical properties of Markforged fabricated continuous carbon fiber reinforced specimens. Four combinations of carbon fiber reinforcement orientations were tested, specifically unidirectional, isotropic, concentric and a combination of isotropic and concentric, with the Markforged Onyx matrix material. Both tensile and flexural properties were measured. To design the UAV wing, a configuration including topology optimized stiffeners with a honeycomb structure was chosen. The wing skin and honeycomb were to be fabricated with the Markforged Onyx material without continuous carbon fiber reinforcements, while the topology optimized sections had continuous fibers. A wing section was fabricated to test the design.

Based on the project to date, the following conclusions were drawn:

- The unidirectional continuous fiber reinforcement orientation was the strongest and stiffest, by far, of the tested orientations. All tested orientations exhibited brittle fracture in tension testing, while the isotropic and concentric combination exhibited the most ductile failure in flexural testing.
- Although the concentric orientation contained only 4 fiber rings and the lowest fiber volume fraction, it had the second best flexural properties. The mechanical property results indicate that mechanical properties of fabricated parts will be highly sensitive to local fiber orientation.
- Wing designs with honeycomb reinforcements are well suited to the Markforged and, more generally, MEX processes. With optimized fiber reinforced regions, resulting wing designs can possess high stiffness to weight ratios.
- The Markforged system makes certain assumptions about depositing fiber reinforcements based on local geometry size and shape that are not necessarily evident to users of the system. Experience is needed to anticipate issues when designing small or narrow regions in which fiber reinforcements are desired.

## Acknowledgement

The authors gratefully acknowledge support from the Singapore DSO under grant DOSCL20019. Support from the Digital Manufacturing and Design Centre at SUTD, funded by the Singapore National Research Foundation, is also acknowledged for access to the Markforged printer.

## References

- [1] I. Gibson, D.W. Rosen, B. Stucker, M. Khorasani, *Additive Manufacturing Technologies*, Third Edition, Springer, 2021. ISBN 978-3-030-56127-7.
- [2] H. L. Tekinalp *et al.*, "Highly oriented carbon fiber-polymer composites via additive

- manufacturing,” *Compos. Sci. Technol.*, vol. 105, pp. 144–150, 2014, doi: 10.1016/j.compscitech.2014.10.009.
- [3] P. Parandoush and D. Lin, “A review on additive manufacturing of polymer-fiber composites,” *Composite Structures*, vol. 182, 2017, doi: 10.1016/j.compstruct.2017.08.088.
- [4] F. Ning, W. Cong, J. Qiu, J. Wei, and S. Wang, “Additive manufacturing of carbon fiber reinforced thermoplastic composites using fused deposition modeling,” *Compos. Part B Eng.*, vol. 80, pp. 369–378, Oct. 2015, doi: 10.1016/J.COMPOSITESB.2015.06.013.
- [5] L. G. Blok, M. L. Longana, H. Yu, and B. K. S. Woods, “An investigation into 3D printing of fibre reinforced thermoplastic composites,” *Addit. Manuf.*, vol. 22, no. May, pp. 176–186, 2018, doi: 10.1016/j.addma.2018.04.039.
- [6] H. Prüß and T. Vietor, “Design for Fiber-Reinforced Additive Manufacturing,” *J. Mech. Des. Trans. ASME*, vol. 137, no. 11, pp. 1–7, 2015, doi: 10.1115/1.4030993.
- [7] S. Kumar and J. P. Kruth, “Composites by rapid prototyping technology,” *Mater. Des.*, vol. 31, no. 2, pp. 850–856, 2010, doi: 10.1016/j.matdes.2009.07.045.
- [8] D. W. Rosen, “Research supporting principles for design for additive manufacturing: This paper provides a comprehensive review on current design principles and strategies for AM,” *Virtual Phys. Prototyp.*, vol. 9, no. 4, pp. 225–232, 2014, doi: 10.1080/17452759.2014.951530.
- [9] M. K. Thompson *et al.*, “Design for Additive Manufacturing: Trends, opportunities, considerations, and constraints,” *CIRP Ann. - Manuf. Technol.*, vol. 65, no. 2, pp. 737–760, 2016, doi: 10.1016/j.cirp.2016.05.004.
- [10] S. Yang, Y. Tang, and Y. F. Zhao, “Assembly-Level Design for Additive Manufacturing: Issues and Benchmark,” *Vol. 2A 42nd Des. Autom. Conf.*, no. August, p. V02AT03A028, 2016, doi: 10.1115/DETC2016-59565.
- [11] G. D. Goh *et al.*, “Characterization of mechanical properties and fracture mode of additively manufactured carbon fiber and glass fiber reinforced thermoplastics,” *Mater. Des.*, vol. 137, pp. 79–89, 2018, doi: 10.1016/j.matdes.2017.10.021.
- [12] L. J. Gibson, “Cellular solids,” *Mrs Bull.*, vol. 28, no. 4, pp. 270–274, 2003.